LOAD FLOW SIMULATION OF A LOW-VOLTAGE PV-BATTERY BASED DC MICROGRID TO SUPPLY SMALL ISOLATED COMMUNITIES

Pedro Ferreira Torres[1] – pedro.ftorres@itec.ufpa.br
José de Arimatéia Alves Vieira Filho[1]– arimateia.eng@outlook.com
Vilson Lima Chaar Junior[1] – vilsonchaar@gmail.com
Leonam Ferreira de Araújo[1] – leo_into@hotmail.com
Samuel Williamson[2] – sam.williamson@bristol.ac.uk
Marcos André Barros Galhardo[1] – galhardo@ufpa.br
João Tavares Pinho[1] – jtpinho@ufpa.br
Wilson Negrão Macêdo[1] – wnmacedo@ufpa.br
[1]Universidade Federal do Pará, Grupo de Estudos e Desenvolvimento de Alternativas Energéticas
[2]University of Bristol, Electrical Energy Management Group

ABSTRACT: This paper presents the modelling and load flow simulation of a low-voltage distribution DC microgrid which is developed in the test area of the Group of Studies and Development of Energy Alternatives (GEDAE-UFPA). This microgrid is intended to serve as a basis for conducting tests of operation modes, power conditioning devices, control strategies, among other possibilities, as well as applications related to low voltage direct current distribution systems, and to validate mathematical models of related processes. The simulated microgrid structure is composed of three photovoltaic generators of 500 Wp each, a battery bank of 4.8 kWh, three charge controllers forming a 24 V DC bus, and load banks distributed along a grid with a total length of 200 m. The modelling of microgrid components are presented in detail, and the load flow study used is derived from the traditional Newton-Raphson power flow algorithm used in AC systems.
Keywords: Modelling, Rural Electrification, Battery Storage and Control, DC Microgrid

1 INTRODUCTION

The search for electricity generation systems that have less impact on the environment and are independent from fossil fuels is growing in several parts of the world. Renewable energy systems are being used in several applications: grid-connected low-voltage distributed systems, centralized PV plants and wind farms, and off-grid battery-powered applications are examples of the various applications being developed worldwide. In this context, the concept of microgrids for energy distribution aims to create a more flexible distribution system. The high penetration of distributed energy sources, especially those with high variability as is the case of PV, can bring problems to the power quality of the distribution grid [1].

Low-voltage DC power distribution systems (LVDC) can be a more efficient alternative to traditional AC systems [2]. The increase in the share of distributed generation sources (in large part by photovoltaic systems) and the use of more efficient electric loads in direct current applications justify the development of this type of microgrid, since it has a reduced number of stages of conversion, making the system more efficient, reliable, and with lower cost [3]. Several other benefits of LVDC can be listed, such as: reduction of line loading and transmission losses (since there is no reactive power flow), reduction in the complexity of power converters, and reduction in losses due to skin effect.

The use of LVDC to supply energy for isolated communities is a feasible alternative to traditional AC systems, as the higher efficiencies in the conversion processes indirectly represent a reduction in the energy storage capacity, which heavily contributes to the overall costs of such systems. Countries like India and Brazil have high demand for such projects, since a significant number of isolated communities without access to electricity could benefit from such systems [4,5]. In this context, this paper proposes a methodology to evaluate the technical feasibility of isolated PV-battery powered LVDC distribution grids for small communities, where it is possible to simulate the battery bank capacity, PV resource and load curves, and also to evaluate the voltage profile at the grid nodes over a day and for several scenarios.

The simulated DC microgrid has been built in the outdoor test area of the Group of Studies and Development of Energy Alternatives (GEDAE-UFPA) laboratory. It is used to perform several studies and tests on this topic, such as: control and energy management strategies, power converters, DC loads, etc. This microgrid is formed by three distributed generation systems, each comprising a 500 Wp PV generator, a configurable lead-acid battery bank (24 V/132 Ah and 48 V/66 Ah) and an MPPT charge controller [6]. Three independent load banks are distributed along the grid, with a maximum power of 200 W, and with configurable load profile (load steps of 40 W), so that a typical load curve for a small community household can be evaluated. To form the grid, 35 mm^2 aluminum multiplexed cables are used, together with 3 poles installed in the laboratory test area. The grid layout is presented in Fig. 1. It is important to highlight that this paper deals only with the simulation results of the proposed system, and real operating results will be considered in a future study.

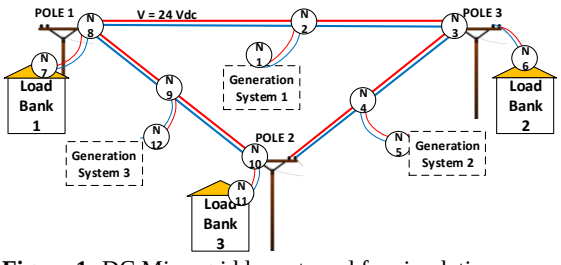

Figure 1: DC Microgrid layout used for simulations.

The following sections describe the modeling of the microgrid components and the algorithm used to evaluate

the power flow. Next, simulation results are presented, considering both real operating load curves and real data of solar resource availability. A discussion of the results is carried out as well as perspectives for future works with the developed microgrid and on the simulation tool.

2 MICROGRID COMPONENTS´ MODELS

The microgrid can be divided into three components to be modeled: the distribution cabling, the generation system, and the load banks. The following items present in detail de model used for each component.

2.1 Grid Cabling

Since no reactive power flow is considered in DC distribution systems (only active power is transmitted), inductive and capacitive effects associated to distribution lines are not present. Hence, only the resistive effects are considered, and the distribution lines are modelled as a single fixed value of resistance.

The resistance value, R, of a conducting line between two grid nodes, n_a and n_b, is obtained from the conductor's electrical resistivity, ρ, the total length, l, and the cross-sectional area, A, as shown in Equation 1.

$$R_{a,b} = \rho . l / A \quad (1)$$

The electrical resistivity is a function of temperature and is usually given considering 20 °C operating temperature, along with a temperature correction factor used to evaluate it for different temperatures. Hence, the distribution line resistance will vary over a day due to temperature changes. However, to simplify calculations, a fixed value for operating temperature of 40 °C was used, which can be considered a worst case scenario. For the aluminum conductors at the considered temperature, ρ = 3.047 x 10^{-8} Ω.m. The total length, l, considers twice the distance between the nodes, since there is both a positive and a negative conductor.

2.2 Generation System

Fig. 2 presents the connections on each generation system.

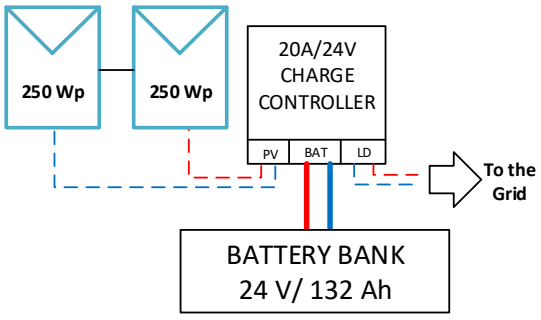

Figure 2: Connections for each generation system.

The charge controller has the function of regulating the charge and discharge of the battery bank, and has maximum power point tracking (MPPT) capability, that ensures the PV generator delivers its maximum available power at a specific operating condition. The charge controller is used to prevent deep discharge of the battery bank, as well as stop any potential overcharging from the PV generation. The output voltage, identified in Fig. 2 as the "LD" terminal, is the same as the battery bank.

The charge controller operates according to two hysteresis curves, shown in Fig 3.

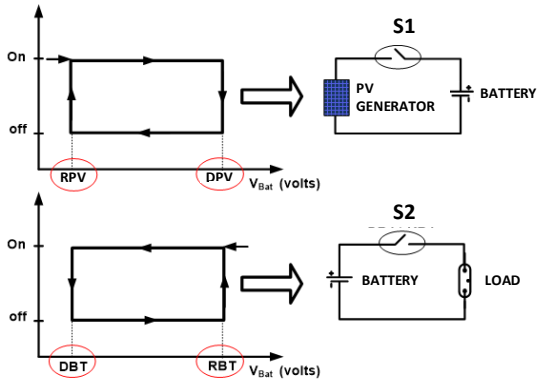

Figure 3: Hysteresis curves for the charge controller (Adapted from [7]).

In the first plot one can identify the regulation to prevent overcharge of the battery bank. The voltage identified as DPV in Fig. 3 is the *Disconnection point of the PV generator*, and when the battery voltage reaches DPV, the charge controller cuts out the PV, as represented by the on/off switch, S1. When the battery starts discharging, the PV generator will be reconnected as battery voltage reaches RPV (*Reconnection point of the PV generator*).

The second plot presents the discharging regulation. The voltage identified as DBT is the *Disconnection point of the battery*, and when the battery voltage reaches DBT, the charge controller cuts out the load (which is connected to the microgrid bus), to prevent deep discharge. This disconnection is represented by the on/off switch, S2, in the figure. When the battery starts recharging, the load is reconnected as battery voltage reaches RBT (*Reconnection point of the battery*).

To model the battery bank, a simple Thevenin equivalent circuit was considered. In this model an ideal voltage source is connected in series with a resistance, R_{BAT}, which represents charge and discharge power losses. The battery open-circuit voltage, V_{OC}, is mainly a function of its state-of-charge, *SoC* [8,9]. For this simulation, a curve $V_{OC} = f(SoC)$ was obtained from the manufacturer's datasheet and embedded in the model.

For the PV generation, real operating data available from PV systems installed in the laboratory was used. The model only needs the output power from the PV generator, since the MPPT algorithm of the converter works for a broad range of voltages (up to 100 V) so that the voltage of the generator is not considered in the calculations. Fig. 4 shows the model used for the generation system.

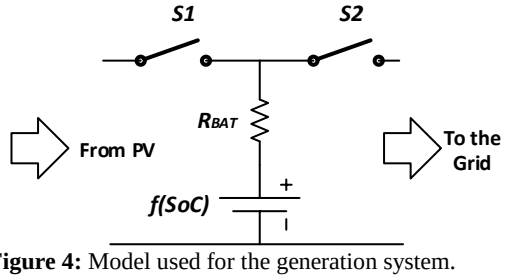

Figure 4: Model used for the generation system.

2.3 Load Banks

Each load bank of the DC microgrid present in GEDAE´s laboratory is currently composed of five resistive lamps rated at 24 V/ 40 W. These lamps can be switched independently, so that each load bank can demand powers of 40, 80, 120, 160 and 200 W. These are considered constant resistive loads, since they can be modelled as pure resistances. The power demanded by a constant resistance load, P_{LD}, is a function of its voltage, V_{LD}, as expressed in equation 2.

$$P_{LD} = V_{LD}^2 / R \quad (2)$$

where R is the load resistance. Each lamp used in the microgrid has a resistance of $24^2/40 = 14.4\ \Omega$.

However, most of the loads found in common household appliances can be considered as constant power loads. This kind of load demands the rated power independently of the voltage at its terminals (provided that the voltage is within the range specified by the manufacturer).

For the power flow studies presented in this paper, only constant power loads were considered. However, constant resistance loads can be easily implemented in the simulation by using equation 2.

3 SIMULATION METHODOLOGY

The simulation algorithm can be divided into three main sections: setup of initial conditions and grid impedance matrix; Newton-Raphson iterative process to evaluate the voltage at each grid node; calculation of the charge at each battery bank. The simulation performs successive power flows with a specified time step, so that a voltage profile over a day can be evaluated. The algorithm flow diagram is shown in Fig. 5.

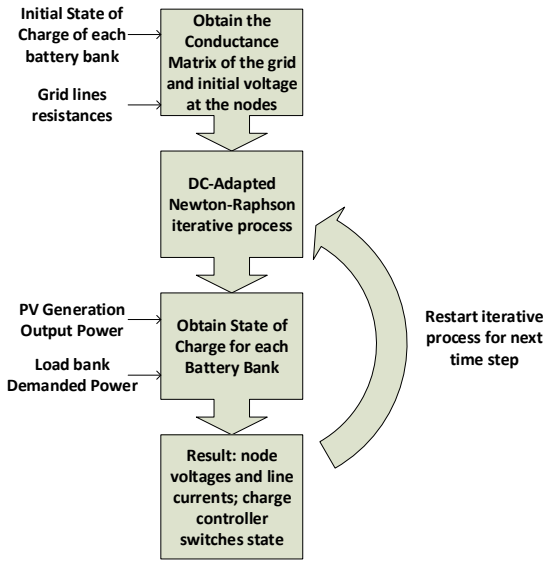

Figure 5: Algorithm workflow.

3.1 Conductance Matrix

In traditional AC power flow, one must obtain the Admittance Matrix of the grid. For DC power flow, the impedance is simplified to resistances (grid cabling is modelled as resistances), and hence, instead of an admittance matrix, Y, a conductance matrix, G, is found [10,11]. Matrix G is formed in a similar manner as the Y matrix. Equation 3 summarizes the calculation process for the elements in matrix G, where k is the number of nodes of the grid, and $R_{i,j}$ is the resistance of the line between grid nodes i and j.

$$G_{i,j} = \begin{cases} -1/R_{i,j}, i \neq j \\ \sum_{n=1,n\neq i}^{k} 1/R_{i,n}, i = j \end{cases} \quad (3)$$

3.2 Newton-Raphson iterative process for DC grids

For DC systems the power flowing at a given bus, i, is expressed in equation 4.

$$P_i = \sum_{j=1}^{k} |V_i|.|V_j|.|G_{i,j}| \quad (4)$$

In matrix form, the Newton-Raphson algorithm for a DC system can be expressed as in equation 5, where $\Delta P_i^{(k)}$ is the residual power at a given bus, i, after an n^{th} iteration, J is the Jacobian matrix, and $\Delta V_i^{(n)}$ is the change in voltage.

$$[\Delta P_i^{(n)}] = [J].[\Delta V_i^{(n)}] \quad (5)$$

The Jacobian matrix is formed as expressed in equation 6.

$$J_{i,j} = \begin{cases} V_j.G_{i,j}, i \neq j \\ \sum_{j\neq i}^{k} V_i.V_j.G_{i,j} + 2.V_i G_{i,j}, i = j \end{cases} \quad (6)$$

3.3 State of Charge for the battery banks

Once the voltages at each node and the current flow at each line are computed, it its time to calculate the *SoC (%)* of each battery bank. This is calculated as expressed in equations 7 and 8.

$$SoC_{i,t} = SoC_{i,t-1} + (P_{FV,i,t} - I_{i,t}.V_{i,t}).\Delta t / V_{i,t} \quad (7)$$

$$SoC_{i,t}(\%) = SoC_{i,t} / C_{BAT} \quad (8)$$

where $SoC_{i,t}$ is the state-of-charge in ampere-hours of a load bank in node i for a given discrete time t, $P_{FV,i,t}$ is the output from the PV generator at the same node and time, $I_{i,t}$ and $V_{i,t}$ are the current and the voltage at node i, Δt is the time step considered in the simulation, and C_{BAT} is the rated battery capacity in ampere-hours.

From the *SoC (%)* it is now possible to apply the *f*(*SoC*) curve obtained from datasheet and derive the voltage of the battery bank. It is then verified if this voltage is within the setpoints of the charge controller, and, if needed, switches S1 or S2 are turned off accordingly.

At this point, the simulation returns to calculate a new power flow for the next time interval.

4 SIMULATION RESULTS

Successive power flow simulations were performed for a day, considering intervals of five minutes. Three buses were considered reference buses for the Newton-Raphson iterative process: N1, N5, and N12 in Fig. 1, which correspond to nodes where the generation systems are connected. The voltage reference adopted for these buses was calculated from the battery model, given an initial known state-of-charge for each battery bank (for the simulation presented in this paper, the initial state of charge for all battery banks is 80 %).

The resistances of the lines for the grid layout presented in Fig. 1 are shown in Table I. Fig. 6 presents the data for PV generation and load profile (both given in watts), for a typical day and with intervals of five minutes for successive simulations of power flow. From Fig. 6 it is possible to see that for this day the maximum output power from PV is close to 350 W at 12 noon, even though the PV generators are rated at 500 Wp. Also, from the generation curve it can be seen that it was a partly cloudy day, with sudden quick drops in the PV generation. From the load point of view, the sudden, repetitive growth that takes about one hour, represents the operation of a freezer, that works at rated power approximately eight hours a day. The load curve presented in Fig. 6 was created considering typical appliances of a household in an isolated community, and a typical use over time of those appliances.

Table I: Resistance of the microgrid lines.

Line (From-To)	2 x Length (m)	Resistance (Ω)
1-2	36	0.031265
2-3	24	0.020843
2-8	24	0.020843
3-4	26	0.022580
3-6	60	0.052109
4-5	78	0.067741
4-10	26	0.022580
8-7	12	0.010422
8-9	20	0.017370
10-11	52	0.045161
9-12	32	0.027791
9-10	20	0.017370

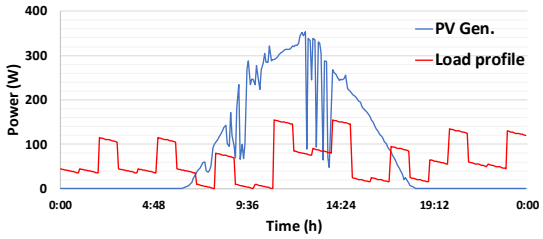

Figure 6: PV generation and load profile for a day with five minutes of data interval.

Fig. 7 shows the voltages at the three load bank nodes, with the results obtained from the power flow algorithm. Two situations were evaluated here: the first, for the implemented 24 V system, and the second for a prospective 48 V bus. Plots in Fig. 7 are given in per unit system (p.u.) with respect to both 24 V, for 24 V bus, and 48 V, for 48 V bus simulations.

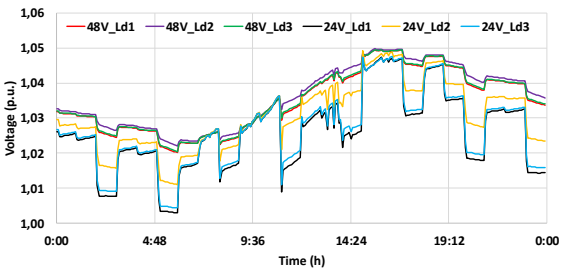

Figure 7: Voltage profile at load buses for 24 V and 48 V.

From Fig. 7 it can be observed that the lower voltages, i.e. higher voltage drops, occur in the 24 V system, which are due to the higher currents circulating at this voltage level. Lower voltages are found in the beginning of the day (around 05h00), when PV generation is not present, the battery bank is partially discharged, and the loads are operating normally (some lamps, freezer, etc.). From an operational point of view, the system will normally supply the loads, since the voltages are always above 1.00 p.u., and thus above rated voltage. The maximum voltage found is around 1.05 p.u., i.e. 5 % above rated voltage, in the afternoon, when PV generation is at its maximum and the battery bank is fully charged.

Fig. 8 shows the SoC (%) for all battery banks. Again, in 48 V system batteries´ SoC is slightly higher that in 24 V. This is explained by the fact that power losses at 24 V are higher, and so more charge is demanded from the batteries. The SoC has a profile similar to the bus voltages, since the battery SoC is related to its output voltage. Fig. 8 shows that around 15h30 the battery banks are fully charged by the PV generation, and start discharging around 17h00, when PV power is decreasing. For the simulated situation, batteries end the day at a higher SoC (around 87 – 90 %) than they started (80 %), but these values tend to oscillate according to PV generation and load profile for a given day.

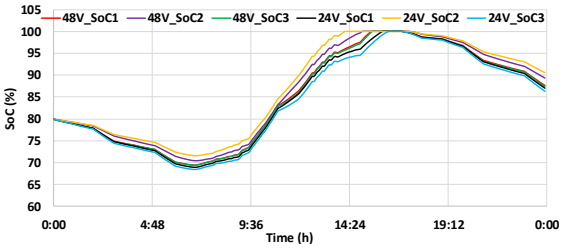

Figure 8: State-of-Charge of all battery banks for 24 V and 48 V systems.

It is important to verify the depth of discharge of the bank for a day, since this factor is one of the main drivers of batteries longevity, and the higher the depth of discharge per discharge cycle (in this case, a day), the lower the number of cycles the battery will be able to hold charge. Special deep-cycle batteries are recommended to be used in such systems, with discharge rates of up to 80 % and a higher guaranteed number of cycles. For the simulated situation, a depth of discharge of 30 % is a common value used for stationary general-purpose batteries.

The power distribution efficiency is a key factor to be evaluated prior to the deployment of a system. System designer must take into consideration the costs associated when selecting the cross section of the distribution cables, bus voltage, etc. Fig. 9 presents the power losses over a day, for both 24 V and 48 V systems. Losses at 24 V are higher and reach up to about 7 % of the total loading of the system. From the data presented in Fig. 9, a detailed economic assessment must be done to evaluate the more feasible configuration, considering both technical and economic perspectives.

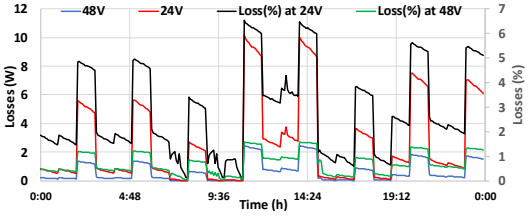

Figure 9: Power losses in distribution lines.

5 CONCLUSIONS

DC distribution microgrids are already being used in specific applications, such as servers and ships, and in most cases present higher efficiency than the traditional AC grids, since they have a reduced number of conversion stages, and their power lines transmit only active power. The increasing number of applications involving distributed generation with renewable energy sources has made DC microgrids gain attention, since efficiency gains are more evident in systems with distributed energy sources and can reduce the complexity of the system and global costs.

This paper has developed a load flow simulation based upon a distributed generation DC microgrid, with PV generators, battery storage and resistive loads. Using models constructed for each component and Newton-Raphson techniques, the system operation for varying PV generation and load has been demonstrated. Two distribution voltages were evaluated, 24 V and 48 V, with the 48 V system showing a 6-times reduction in loss during times of high load, when compared to a 24 V system.

Simulation tools such as presented in this paper are an important way to visualize system performance for several scenarios, helping system designer in the project and development stage. Further work will compare real operating data from the DC microgrid already installed in GEDAE´s laboratory, and improve the simulation tools from this data. Also, other simulations are under way, to evaluate system stability and other operating and control strategies. Also, other works on this simulation tool will include improvements in battery modeling, so that aging processes can be considered during simulations, as well as the implementation of demand-side management and droop control voltage regulation.

REFERENCES

[1] Jenkins, N., Allan, R., Crossley, P., Kirschen, D., Strbac, G. *Embedded Generation*. IET Power and Energy Series, 2008.

[2] Kumar, D., Zare, F., Ghosh, A. "DC Microgrid Technology: System Architectures, AC Grid Interfaces, Grounding Schemes, Power Quality, Communication Networks, Applications and Standardizations Aspects", *IEEE Access*, June 2017.

[3] Elsayed, A., Mohammed, A. A., Mohammed, O. A. "DC Microgrids and Distribution systems: An overview", *Electric Power System Research*, no. 119. 2015.

[4] Nascimento, R. L., "Energia Solar no Brasil: Situação e Perspectivas", *Consultoria Legislativa*. Tech. Report, March 2017.

[5] Jhunjhunwala, A., Lolla, A., Kaur, P. "Solar-DC Microgrid for Indian Homes: A transforming power scenario", *IEEE Eletrification Magazine*, June 2016.

[6] Torres, P. F.; Vieira Filho, J. A. A.; Williamson, S. J.; Chaar Junior, V. L.; Pinho, J. T.; Galhardo, M. A. B.; Macêdo, W. N.; "Concepção de Estrutura Laboratorial para Realização de Estudos em Microrrede em Corrente Contínua de Baixa Tensão", In. Proc. VII Congresso Brasileiro de Energia Solar, Gramado, Brazil. 2018.

[7] Oliveira, L.G. M, "Estratégias de Controle de Carga e Descarga em Sistemas Fotovoltaicos Domiciliares", M.Sc. dissertation, Universidade de São Paulo, Brazil, 2005.

[8] Coleman, M; Lee, C. K.; Zhu, C.; Hurley, W. G.; "State-of-Charge Determination from EMF Voltage Estimation: Using Impedance, Terminal Voltage, and Current for Lead-Acid and Lithium-Ion Batteries", *IEEE Transactions on Industrial Electronics*. Vol. 54, No. 5. October 2007.

[9] Rana, M. J.; Abido, M. A.; "Energy management in DC microgrid with energy storage and model predictive controlled AC–DC converter", *IET Generation, Transmission & Distribution, Special Issue: Smart Grid Voltage Control.* Vol. 11, Iss. 15, pp. 3694-3702. 2017.

[10] Jayaranthna, C.; Binduhewa, P.; Ekanayake, J.; Wu, J. "Load Flow Analysis of Low Voltage dc Networks with Photovoltaic", In. Proc. 9th International Conference on Industrial and Information Systems, ICIIS 2014, art. no. 7036566, 2015.

[11] Farooq, R.; Mateen, L.; Ahmad, M.; Akbar, S. Q.; Khan, H. A.; Zaffar, N. A.; "Smart DC Microgrids: Modeling and Power Flow analysis of a DC Microgrid for off-grid and weak-grid connected communities", In. Proc. (2014) Asia-Pacific Power and Energy Engineering Conference, APPEEC, 2015-March (March), art. no. 7066139.